10º Congreso de Exploración y Desarrollo de Hidrocarburos
Simposio de Evaluación de Formaciones: Maximizando la eficiencia a través de la innovación

SPECTRAL GAMMA-RAY LOGGING OF CERRO BALLENA ANTICLINE, SANTA CRUZ PROVINCE: AN OUTCROP ANALOGUE TO SUBSURFACE CHARACTERIZATION AND WELL-LOG CORRELATION OF FLUVIAL SANDSTONE RESERVOIRS

José Matildo Paredes[1], Sergio Roberto Giordano[2], Mauro Nicolás Valle[3], José Oscar Allard[1], Nicolás Foix[3]

1: U.N.P.S.J.B, paredesjose@yahoo.com, joseoallard@yahoo.com.ar

2: SINOPEC ARGENTINA E&P INC, sergio_giordano@sinopecarg.com.ar

3: CONICET- U.N.P.S.J.B, nicofoix@hotmail.com

Keywords: **modelado estocástico, ambientes deposicionales, relación hierro/azufre**

RESUMEN

Perfiles de rayos gamma espectral del anticlinal del Cerro Ballena, provincia de Santa Cruz: un análogo de afloramiento para la caracterización de subsuelo y correlación por perfiles de pozo de reservorios de areniscas fluviales.

Los perfiles de rayos gamma espectral (SGR) de afloramiento son útiles para la caracterización de análogos de reservorios y para mejorar las correlaciones de perfiles de pozo en subsuelo. Este trabajo analiza afloramientos de la Formación Bajo Barreal (Cretácico superior) en el anticlinal del Cerro Ballena (provincia de Santa Cruz), combinando mediciones de SGR con datos litológicos y mineralógicos. Los afloramientos analizados muestran, en la base, canales pequeños y con baja interconectividad dentro de limoarcillitas silicoclásticas (Sección A, 185 m) que evolucionan verticalmente a canales de mayor escala y mayor conectividad, intercalados con facies finas de planicie de inundación de naturaleza volcaniclástica (Sección B, 270 m). Se realizaron tres perfiles de SGR en una sección de 380 m de potencia usando una separación vertical entre mediciones de 50 centímetros. En los afloramientos se reconocieron trenes verticales de reducción de K y GR total hacia la parte alta de la Sección A, asociados a lavado de K durante la meteorización, con incremento simultáneo del contenido de caolinita, que en conjunto implican un incremento en la tasa de meteorización química hacia arriba en la Sección A. Los trenes de K y GR total identificados en la Sección A permitieron correlacionar el registro del cerro Ballena con perfiles de GR del yacimiento Cerro Wenceslao, en donde los ciclos identificados presentan similar potencia. Complementariamente, utilizando estimaciones paleohidráulicas en el relleno de 41 canales de las secciones A y B, se reconoció incremento en la profundidad de flujo y del ancho del canal, aumento de caudal y del tamaño del área de drenaje de los ríos incluidos dentro de la Sección B, confirmando de manera independiente mayor disponibilidad de agua en el sistema fluvial, así como condiciones de clima más húmedo en la Sección B. Las metodologías utilizadas han demostrado un origen climático a los trenes verticales observados en el perfil SGR, y permiten además establecer que las variaciones observadas en el apilamiento de los canales entre la Sección A y la Sección B están asociadas a cambios climáticos hacia clima más cálido y húmedo.

INTRODUCTION

Spectral gamma ray (SGR) logs are widely used in the oil industry to identify facies, for subsurface correlation and sequence-stratigraphic interpretation (Rider 1999; Catuneanu 2006). Outcrop SGR combined with facies analysis and geochemistry proved to be useful for paleoclimatic reconstructions (Myers and Wignall 1987; Ruffell *et al.* 2003; Ghasemi-Nejad *et al.* 2010), to highlight relationships between texture, composition and provenance (North and Boering 1999; Corbeanu *et al.* 2001; Evans *et al.* 2007; Šimíček *et al.* 2012), and for stratigraphic analysis (Myers and Bristow 1989; Parkinson 1996; North and Boering 1999). Outcrop SGR also allow to correlate outcrop sections with wire-line data using the vertical variation of K, U and Th (Hampson *et al.* 2005; Keeton *et al.* 2015). Much of these studies are concentrated in carbonate strata, where the dilution of terrigenous Th and K in marine calcium carbonate is interpreted as a proxy for marine or continental influence (Postma and Ten Veen 1999; Lüning *et al.* 2004; Hladil *et al.* 2006; Babek *et al.* 2007, 2013). In sedimentary successions, potassium is found mainly in K-feldspar, micas and illitic clays, whereas thorium is concentrated in sand and silt-sized heavy minerals, phosphates or adsorbed and concentrated in clays (Ruffell *et al.* 2003). Uranium is hosted by heavy minerals but can also be enriched in anoxic organic-rich sediments (Myers and Wignall 1987; Anderson *et al.* 1989). Higher gamma ray counts are commonly attributed to mudstone. The presence of K-bearing illite, I/S mixed layer clays, sericite and the tendency of U and Th to adsorb on the surface of clay minerals and organic matter is common in fine-grained facies (Rider 1999; Lüning *et al.* 2004). Low gamma-ray counts are typical for sandstone and conglomerate facies due to the dilution effect of non-radioactive quartz, carbonate cement and pore space (Rider 1990, 1999). However, these grain size related effects can be complicated by mineralogy or diagenesis. Many siliciclastic facies can include variable amounts of K-bearing grains (e.g. K-feldspars, albite and micas) in the sand fraction, Th- and U bearing heavy minerals (zircon, apatite, monazite, rutile, davidite, brannerite, etc.) in the sand-to-silt fraction, K-bearing phyllosilicates (illite, glauconite and smectite), and the organic matter (cf. Durrance 1986; Doveton 1994; Lindqvist 1997; Jain *et al.* 1998; Svendsen and Hartley 2001). Although GR and SGR well-logs are commonly used for correlation and in sequence stratigraphic analysis (Catuneanu 2006), attempts to correlate outcrops SGR logs with facies analysis on large-scale depositional systems are not common (Aigner *et al.* 1995; Evans *et al.* 2007), presumably due to usually poorly predictable composition effects of the most of siliciclastic sediments. In the Golfo San Jorge basin, SGR well-logs are frequently recorded during drilling, although their utility as a proxy for grain size or lithology is not concluding due to the variable incorporation of radio-elements in volcaniclastic components delivered to the fluvial systems (Acuña *et al.* 2011).

The Golfo San Jorge Basin, which is located in Central Patagonia, has produced approximately 10 billion barrels of oil (1,500 million m^3) during its more than 100 years of development history. With more than 40.000 drilled wells, it currently provides nearly 50% of all liquid hydrocarbons and 13% of all gas of Argentina's production (Secretaría de Energía 2016). Up to 90% of these hydrocarbons are recovered from fluvial channels in the Upper Cretaceous Bajo Barreal Formation, and subsurface equivalents. The exposures of the Bajo Barreal Formation in the Cerro Ballena anticline (Santa Cruz province) provide a good subsurface fluvial analog because it is reservoir scale (2.5 km wide x 385 m thick) and have well exposed facies relationships. Previous research in the Cerro Ballena anticline have identified a siliciclastic section with isolated channels at base (Section A, 180 m thick sensu Figari *et al.* 1998) covered by densely-stacked channel belts encased in a fine-grained volcaniclastic floodplain (Section B, 182,5 m thick sensu Figari *et al.* 1998). Those results were expanded by Bridge *et al.* (2000), where qualitative and quantitative information of fluvial sandbodies and floodplain facies was presented. An update of the channel belt characteristics and fluvial style variations of the Bajo Barreal Formation at Cerro Ballena anticline was presented in Paredes *et al.* (this congress).

In this paper, we provide results of detailed outcrop SGR logging of the two distinctive lithological packages with different stacking styles that occur within the Bajo Barreal Formation at Cerro Ballena anticline. The field data also provide paleohydraulical parameters derived from measurements of cross-bed set thickness, and it is supplemented with laboratory XRD measurements of fine-grained mudstones aimed at tracing climatically controlled compositional changes.

GEOLOGICAL FRAMEWORK

The Bajo Barreal Formation (Lesta and Ferello 1972) was deposited in an endorheic basin over an area exceeding 150000 km^2. Its maximum thickness is up to 1300 m in the subsurface (Fitzgerald *et al.* 1990), whereas at outcrop it reaches 670 meters in the Codo del Senguerr anticline (Paredes *et al.* 2016). Due to its wide distribution, the interpretations of its environment changes across the basin, being identified lacustrine fans, volcaniclastic alluvial fans, meandering and braided rivers, and ephemeral rivers (Brown *et al.* 1982; Barcat *et al.* 1989; Hechem *et al.* 1990; Legarreta *et al.* 1993; Rodriguez 1993; Hechem 1997; Georgieff and Benedetto 2005; Georgieff *et al.* 2009; Umazano *et al.* 2008). Outcrop analysis along most of the San Bernardo fold belt recognized a Lower Member and an Upper Member, distinction based in the floodplain composition and scale of sandbodies. The Lower Member is characterized by channeled sandstones interbedded with fine grained (very fine sand-size) tuffaceous strata, whereas the Upper Member is composed of larger-scale, isolated channel sandbodies surrounded by grey siltstones and siliciclastic mudstones (Figari *et al.* 1990; Umazano *et al.* 2008). Although most sedimentological studies at outcrops indicate the occurrence of fluvial systems with large discharge variation or ephemeral rivers (Hechem 1997; Umazano *et al.* 2008; Paredes *et al.* 2016), a palynological assemblage recovered in the subsurface of the basin (Archangelsky *et al.* 1994) from the Lower Bajo Barreal Formation indicate humid, continental mild to warm climate.

The Cerro Ballena anticline constitutes the western limb of a faulted, plunging anticline, the axial trace of which is oriented NNW–SSE. Cerro Ballena is bounded to the west by a reverse fault, and to the south by the Deseado River. The strike of the strata is N110ºE to N130ºE, and dips range from 3° to 50° (Fig. 1). In the area of the Cerro Ballena anticline, Figari *et al.* (1998) identified three main lithological packages defined according to the occurrence of discontinuities, lithofacies types and stacking patterns, named A, B and C in ascending order. The Sections A and B are exposed in the core and western limb of the Cerro Ballena (Figs 2, 3 and 4) and constitute the main subject of this research, while the Section C is partially identified in the southern plunge of the anticline and mainly southward of the Deseado river (Figari *et al.* 1998). The Section A is 180 m thick and it consists of pale green and yellow siltstones interbedded with small-scale channel fills up to 2.5 m thick, interpreted as unconfined sheetfloods and crevasse splays, ephemeral currents and distal mudflows arriving to a low-energy environment with limited paleosol development. The Section B is a 300 m thick succession that starts at the base of the first level of red-colored tuffaceous mudstone exposed in the western limb of the Cerro Ballena anticline; it is interpreted as the record of meandering rivers, with well-preserved overbank deposits and occasional provision of ash-fall beds (Figari *et al.* 1998). The overlying Section C is about 300 m thick and its base is correlatable with uppermost levels of Section B of the western limb of the anticline. It consists of green to grey mudstones with interbedded sandstones and has been interpreted associated to sheetflood processes and deposition from distal mudflows in a barreal environment (Figari *et al.* 1998).

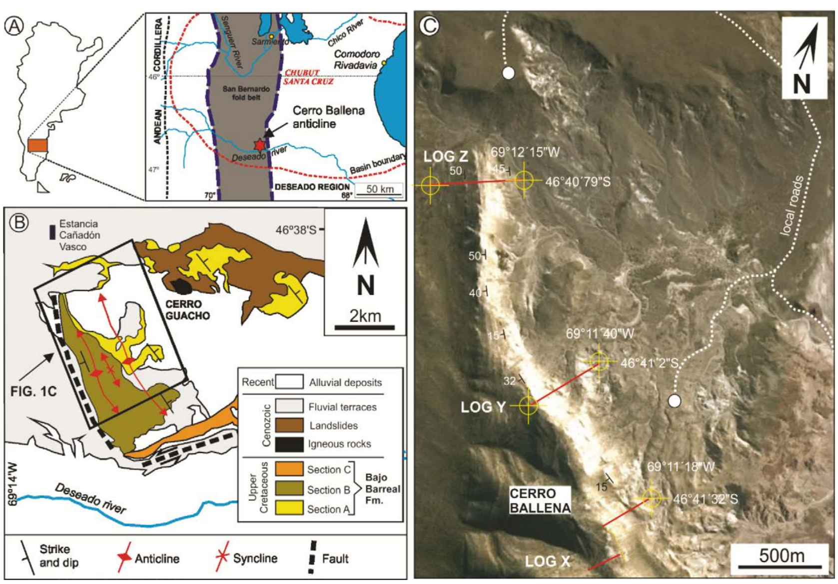

Figure 1. A) Location map of the Golfo San Jorge Basin in central Patagonia, Argentina, with indication of the location of the Cerro Ballena anticline (star). B) Simplified geological map of the area of the Cerro Ballena anticline, southwestern Golfo San Jorge Basin (after Figari *et al.* 1998). C) GoogleTM image of the Cerro Ballena anticline, with location of the sedimentary logs (Logs X, Y and Z). Local roads are indicated as dotted lines.

METHODOLOGY

Three outcrop gamma-ray logs (Log X, Log Y and Log Z in Fig. 1C) were obtained along the cliff face, through approximately 385 m of the Bajo Barreal Formation, with measurements using a vertical separation of 50 centimeters. Weathering and local rubble coverage of the fine-grained sections led to the need for extensive trenching to achieve unweathered surface exposures. The natural radioactivity of the rock units was measured with a portable device (RS-125), which allows to show the result as the numerical value recorded by the spectroscope either as counts per minute over the determined sample time or as the content of radioactive elements in the sample (% of K_2O or ppm of U and Th). A counting time of 2 minutes was adopted during the fieldwork. The mineralogical compositions and clay identification of ten fine-grained samples were determined via x-ray diffraction (XRD).

We also analyse the vertical evolution of several parameters, including flow depth, average and bankfull width, paleoslope and drainage area utilizing set thickness of cross beds, measured within eleven fluvial channels of Section A, and in thirty channels of Section B. The number of cross sets measured in each data included in this dataset ranges from 4 to 11. The scaling relationships used in this research, their sources and descriptions, are presented in Table I.

Parameter	Equation	References
Mean dune heigth (h_m)	(1) h_m=5,3β+0,001β^2 ; β≡Sm/1,8 (Sm=mean cross-set)	Leclair and Bridge (2001); Leclair (2002)
Mean Flow Depth (d)	(2) d = (8.0 ± 2.0)h_m	Bridge and Tye (2000)
Channel Width (W_c)	(3) Wc=8,88dm^{1,82}, dm=0.5d	Bridge and Mackey (1993)
Average daily discharge (Qm)	(4) Qm=v.A	
Mean bankfull channel depth (d_b)	(5) d_b = 0.6M$^{0.34}$Qm$^{0.29}$	Schumm (1968)
Bankfull channel width (W_b)	(6) W_b= 8.9$d_b^{1.40}$	Leeder (1973)
Average daily discharge (Qm) (2nd method)	(7) Qm = 0.027$w_b^{1.69}$	Osterkamp and Hedman (1982)
Paleoslope (S)	(8) S= 60M$^{-0,38}$Qm$^{-0,32}$	Schumm (1968)
Mean bankfull water discharge (Qb)	(9) Qb= 4.0$A_b^{1.21}$S$^{0.28}$	Williams (1978)
Drainage area (A_d) (in km^2)	(10) Qb= Ad$^{0.75}$	Leopold *et al.* (1964)
Principal stream length (L)	(11) L=1.4Ad$^{0.6}$	Leopold *et al.* (1964)

Table I. Paleomorphological parameters and equations.

SPECTRAL GAMMA-RAY LOGS AT OUTCROPS

The three outcrop SGR logs from the cerro Ballena anticline (Fig. 1C) are shown in Figures 2-4, together with the sedimentary log.

Facies distribution of SGR data

SGR data from the Cerro Ballena anticline shows moderately high radioactivity (dose rate: 45.6-180 nGy/h; Total GR: 42.4-175 ppm) and concentration of K (0.4-3.5%), U (0-17.6 ppm) and

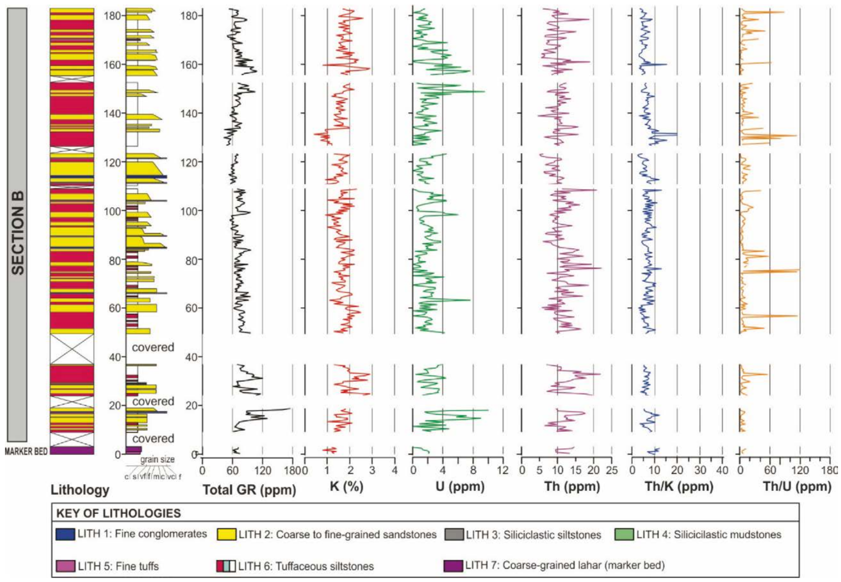

Figure 2. Sedimentary log and gamma ray data for Log X (183 m), covering the southern area of the Cerro Ballena Anticline (location in Fig. 1C). The diagram shows, from left to right, lithology, grain size, and then the gamma-ray data: Total GR (ppm), potassium (K %), uranium (ppm U), thorium (Th ppm), Th:U ratio, and Th:K ratio. Unexposed sections hidden beneath talus, where SGR data could not be collected, are shown as gaps. The main subdivisions of Section A, physically correlated and walked out along the exposures, are indicated.

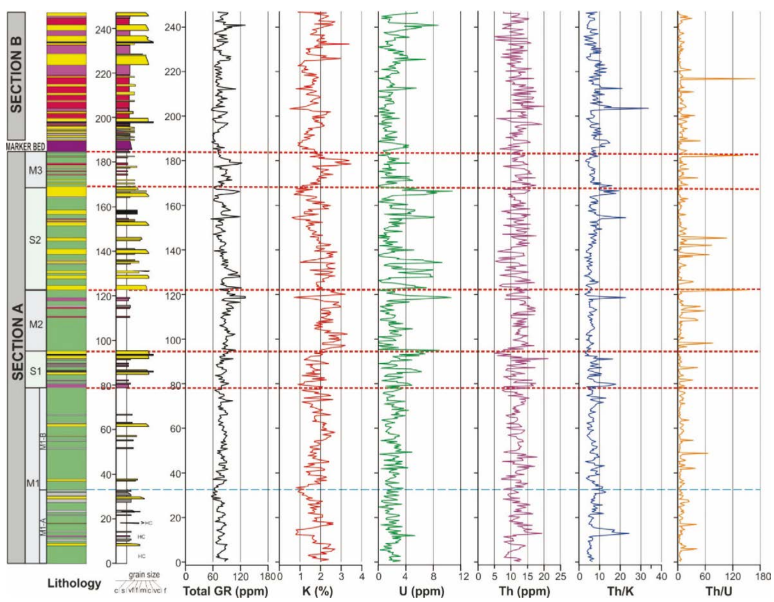

Figure 3. Sedimentary log and gamma ray data for Log Y (247 m). Location in Fig. 1C. The diagram shows, from left to right, lithology (code facies as in Fig. 3), grain size, and then the gamma-ray data: Total GR (ppm), potassium (K %), uranium (ppm U), thorium (Th ppm), Th:U ratio, and Th:K ratio.

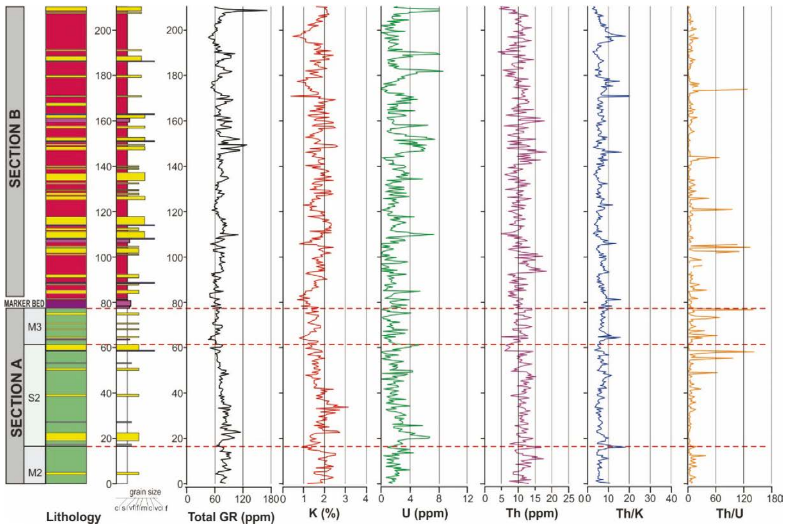

Figure 4. Sedimentary log and outcrop gamma ray data for Log Z (210 m). Location in Fig. 1C. The diagram shows, from left to right, lithology (code facies as in Fig. 3), grain size, and then the gamma-ray data: Total GR (ppm), potassium (K %), uranium (ppm U), thorium (Th ppm), Th:U ratio, and Th:K ratio.

Th (4.2-22.1 ppm). In order to simplify the statistical analysis of data we have grouped the seventeen lithofacies identified during the fieldwork (see Paredes *et al.* this congress) in seven major facies categories, as follow: LITH1: Conglomerates, LITH2: Sandstones, LITH3: Siliciclastic siltstones, LITH4: Siliciclastic mudstones, LITH5: Fine-grained tuffs, LITH 6: Tuffaceous siltstones, and LITH 7: Coarse-grained lahar. Moreover, we have grouped the data obtained from Logs X, Y and Z based in their inferred palaeoenvironment, as follow: FA1: fluvial channels; FA2: proximal floodplain; FA3 distal floodplain (epiclastic, Section A); FA4 distal floodplain (volcaniclastic, Section B), and FA5: coarse-grained lahar (the distinctive marker bed near the base of Section B).

A correlation matrix for total GR and the three radioactive components is shown in Figure 5 for the overall data, and for the seven main facies categories (LITH 1 to LITH 7). As U (ppm) and K (%) values are relatively low, the correlation matrix use count per minute data, to reduce the statistical noise.

The Total GR log is dominated by the potassium content (Fig. 5) shown by the high correlation between potassium log and the total counts (r=0.78) although U shows highly significative correlations with total counts (r=0.75), and Th display the less significant relation with total counts (r=0.37). The generally weak correlation between elements (Th-K r=0,20; Th-U r=0,17; U-K r=0.35) suggests that the sum radioactivity is sourced from multiple mineral carriers and, implies a broad compositional variation within the Bajo Barreal Formation. In conglomerates and sandstones, U and Total GR show correlations highly significative (sandstones r=0,83; conglomerates r=0,90), evidencing that the main contributor to the total radioactivity is the U element (Fig. 5). High-radioactivity in conglomerates and sandstones is relatively common in the geological record, being mainly attributed to the contents of mica, K-feldspars, lithic fragments and

CERRO BALLENA ANTICLINE n=1293	K_{sgr}	U_{sgr}	Th_{sgr}	GR Total
K_{sgr}	1.00			
U_{sgr}	0.35	1.00		
Th_{sgr}	0.20	0.17	1.00	
GR Total	0.78	0.75	0.37	1.00

LITH 1 - CONGLOMERATES n=12	K_{sgr}	U_{sgr}	Th_{sgr}	GR Total
K_{sgr}	1.00			
U_{sgr}	0.76	1.00		
Th_{sgr}	0.10	-0.07	1.00	
GR Total	0.88	0.90	0.10	1.00

LITH 2 - SANDSTONES n=230	K_{sgr}	U_{sgr}	Th_{sgr}	GR Total
K_{sgr}	1.00			
U_{sgr}	0.51	1.00		
Th_{sgr}	0.14	0.13	1.00	
GR Total	0.82	0.83	0.29	1.00

LITH 3 - SILICICLASTIC SILTSTONES n=179	K_{sgr}	U_{sgr}	Th_{sgr}	GR Total
K_{sgr}	1.00			
U_{sgr}	0.54	1.00		
Th_{sgr}	0.22	0.19	1.00	
GR Total	0.79	0.87	0.37	1.00

LITH 4 - SILICICLASTIC MUDSTONES n=397	K_{sgr}	U_{sgr}	Th_{sgr}	GR Total
K_{sgr}	1.00			
U_{sgr}	0.15	1.00		
Th_{sgr}	0.13	0.24	1.00	
GR Total	0.78	0.54	0.37	1.00

LITH 5 - FINE-GRAINED TUFFS n=74	K_{sgr}	U_{sgr}	Th_{sgr}	GR Total
K_{sgr}	1.00			
U_{sgr}	0.16	1.00		
Th_{sgr}	0.08	0.51	1.00	
GR Total	0.53	0.83	0.46	1.00

LITH 6 - TUFFACEOUS SILTSTONES n=383	K_{sgr}	U_{sgr}	Th_{sgr}	GR Total
K_{sgr}	1.00			
U_{sgr}	0.36	1.00		
Th_{sgr}	0.36	0.43	1.00	
GR Total	0.79	0.71	0.57	1.00

LITH 7 - COARSE GRAINED LAHAR n=18	K_{sgr}	U_{sgr}	Th_{sgr}	GR Total
K_{sgr}	1.00			
U_{sgr}	0.61	1.00		
Th_{sgr}	-0.08	-0.19	1.00	
GR Total	0.79	0.72	0.02	1.00

Figure 5. Correlation matrix for radioactive elements determined by outcrop SGR data (Logs X, Y and Z), and for the assigned facies categories.

heavy minerals (Rider 1999). In our study area, high values of U in conglomerates and sandstones are likely associated to diagenetical processes or to fluid migration, and not to the occurrence of heavy minerals in the fine-grained matrix, due to the low Th content observed in conglomerates and sandstones. A likely source of radioactivity could be the occurrence of hydrocarbons in the matrix, due to the common oil staining of the channelized sandstones at outcrops.

The statistical distribution of Total GR, K, U and Th counts in the facies categories are presented in Table II. Although the statistical overlapping is important, some trends have been observed using SGR data: (i) Th values show increasing values from conglomerates to mudstones, but the differences (Th 5 ppm) is insufficient to use this values as a basis for facies discrimination; (ii) U values show decreasing values from conglomerates to mudstones, a trend less defined than for Th element; (iii) the distinctive marker bed (LITH 7) located close to the base of Section B (sensu Figari *et al.* 1998) show very low values of K and total GR. Moreover, distal volcaniclastic components of the floodplain (FA4 and FA5, see Table II) show lower counts in Total GR than fine-grained siliciclastic floodplain facies (FA3).

Although some trends can be identified using concentration of U in sandstones and the Th distribution evidence some relation with grain size (Table II), the large overlap of values and small diferences between facies categories do now allow to make lithological distinction using basic statistics. To obtain a more robust statistical approach, an experimental model based in simple

(A) LITHOLOGY/GRAIN SIZE	n	Total GR (ppm) mean (StD)	K (%) mean (StD)	U (ppm) mean (StD)	Th (ppm) mean (StD)	Th/K mean (StD)	Th/U mean (StD)
LITH 1: Conglomerates	12	75.5 (11.8)	1.9 (0.3)	2.6 (1.8)	8.8 (2.2)	4.8 (1.3)	6.1 (5.7)
LITH 2: Sandstones	230	80 (16)	1.7 (0.4)	**3.5 (2.4)**	9.9 (2.9)	6.1 (2.5)	6.4 (14.7)
LITH 3: Siliciclastic siltstones	179	74.4 (17.1)	1.7 (0.4)	2.6 (2.3)	10.2 (2.7)	6.5 (2.4)	7.7 (13.5)
LITH 4: Siliciclastic mudstones	397	80 (10.2)	1.9 (0.5)	1.9 (1.2)	12.2 (2.3)	6.8 (2.5)	11.4 (17.4)
LITH 5: Fine-grained tuffs	74	71.5 (11.8)	1.4 (0.4)	2.2 (1.5)	11.8 (2.4)	9.0 (4.3)	7.6 (6.6)
LITH 6: Tuffaceous siltstones	383	72.6 (12.5)	1.7 (0.4)	1.7 (1.2)	11.6 (2.8)	7.3 (3.2)	12.6 (21.1)
LITH 7: Coarse-grained lahar (marker bed)	18	66.4 (6.8)	**1.1 (0.2)**	2.1 (1.4)	11.2 (2.5)	10.1 (2.7)	8.1 (11.4)

(B) FACIES ASSOCIATION	n	Total GR (ppm) mean (StD)	K (%) mean (StD)	U (ppm) mean (StD)	Th (ppm) mean (StD)	Th/K mean (StD)	Th/U mean (StD)
FA 1: Fluvial channels	290	78.8 (17.8)	1.7 (0.4)	3.5 (2.5)	9.5 (2.7)	5.8 (2.3)	5.5 (10.6)
FA 2: Proximal floodplain	156	75.2 (13.8)	1.6 (0.4)	2.3 (1.7)	11.3 (2.8)	7.4 (3.1)	10.5 (20.9)
FA 3: Distal, epiclastic floodplain	649	77.5 (11.4)	1.8 (0.5)	1.9 (1.2)	12.2 (2.5)	7.2 (3.0)	11.9 (18.8)
FA 4: Distal, volcaniclastic floodplain	180	69.6 (11.4)	1.6 (0.4)	1.9 (1.3)	11.0 (2.3)	7.6 (3.2)	10.4 (16.3)
FA5: Coarse-grained lahar (marker bed)	18	66.4 (6.8)	1.1 (0.2)	2.1 (1.4)	11.2 (2.5)	10.1 (2.7)	8.1 (11.4)

(C) STRATIGRAPHIC UNIT	n	Total GR (ppm) mean (StD)	K (%) mean (StD)	U (ppm) mean (StD)	Th (ppm) mean (StD)	Th/K mean (StD)	Th/U mean (StD)
Section A	528	80.1 (12)	1.8 (0.5)	2.3 (1.7)	11.8 (2.5)	6.9 (2.8)	10.3 (17.1)
Section B	765	73.7 (14.2)	1.7 (0.4)	2.3 (1.8)	10.9 (2.9)	7.0 (3.0)	9.8 (17.4)

Table II. Mean values for total radioactivity, potassium (% K), uranium (ppm U) and thorium (ppm Th) contents of Log X, Log Y and Log Z for A) facies categories, B) facies association, and C) Stratigraphic unit within the Bajo Barreal Formation. Mean Th/K and Th/U ratio are also indicated. StD, standard deviation. Red boxes indicate anomalous values, and triangles represent grainsize-related tendencies.

variance analysis (ANOVA) and Machine Learning algorithms will be presented in a separate contribution (Castillo Gamarra *et al.* this congress).

Outcrop-subsurface correlation

The lateral correlation of the outcrop SGR logs (Fig. 6) use as datum the distinctive volcaniclastic marker bed that separates the Section A and B of the Bajo Barreal Formation (see Paredes *et al.* this congress). As mentioned, Section A can be subdivided in several major zones of tens of meters according to its sandstone content (indicated as M1, S1, M2, S2 and M3 in ascending order). The major subdivisions of Section A can be also traced confidently between the SGR logs with minimum thickness variations, evidencing a cake-layer distribution of the main packages. Moreover, outcrop SGR data were confidently correlated with wells CW.x-3002 and CW.x-3003 of Cerro Wenceslao oilfield using two distinctive log motifs identified in Section A. In the lowermost part of the fine-grained succession of Section A, a subtle upward reduction of GR values in subdivision M1-B can be compared with an equivalent GR motif identified in the CW.x-3003

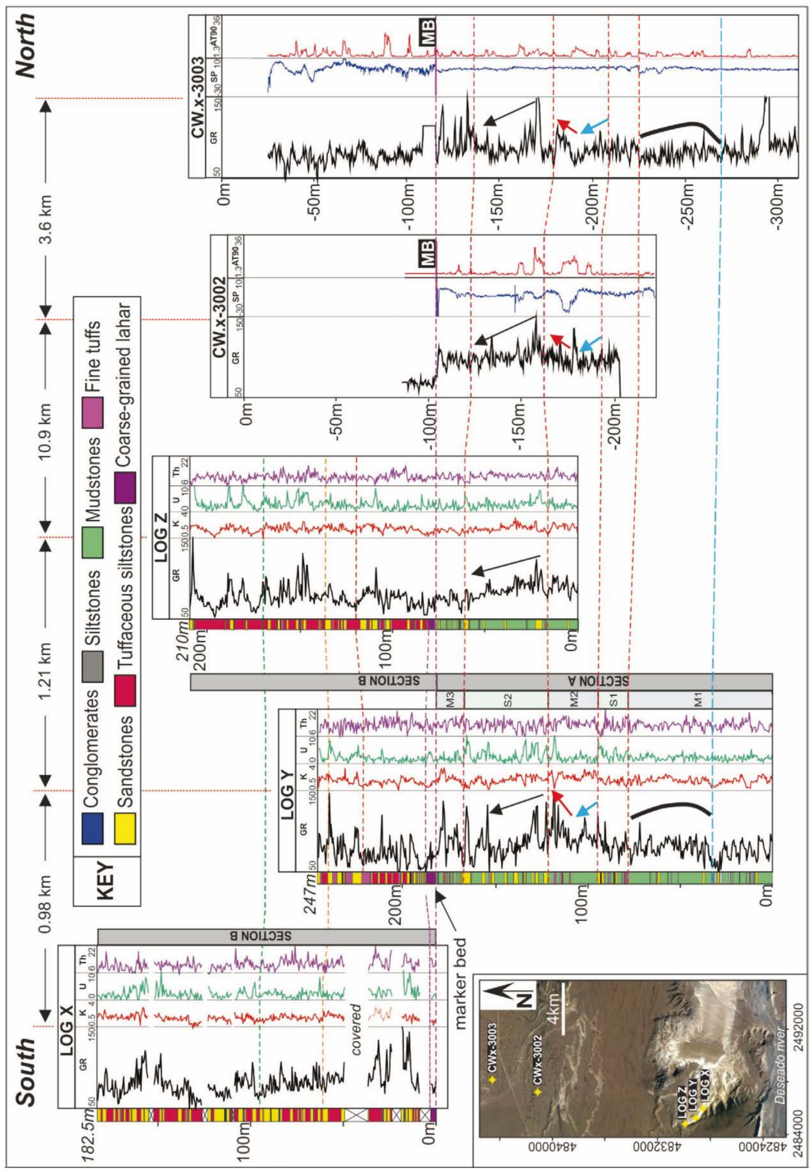

Figure 6. SGR-log stratigraphic correlation between outcrop gamma-ray logs obtained in the Cerro Ballena anticline (Logs X, Y and Z) and wells CW.x-3002 and CW.x-3003 in the Cerro Wenceslao oilfield. The horizontal datum corresponds to the tuffaceous marker bed (MB) located near the base of Section B. The lithologies described in the field are indicated to the left of the GR logs. Major sub-divisions and distinctive log pattern observed in Section A and B are also represented. Notice upward decreasing in Total GR and K counts throughout S2 and M3 packages of Section A, which can be confidently identified in the subsurface. See inset map for location. SP=spontaneous potential, AT90= deep resistivity.

well log. A second distinctive GR motif occurs in the S2 subdivision (Fig. 6), associated to an upward reduction in both GR and K values.

Due to the long distance (up to 12 km in a straight line) that separates the Cerro Ballena exposures and the CW.x-3003 well, we suggest that the origin of this upward decreasing K trend could be due to an increase in the chemical weathering rate and associated leaching of K in the early diagenesis, evidencing more humid climate conditions upward of Section A (see below). Depletion of K has been commonly mentioned as an indicator of high weathering rate due to its solubility in aqueous solution, usually water movement (Osmond and Ivanovich 1992; Rosholt 1992). On the other side, lateral correlation of SGR-derived Logs X, Y and Z in Section B is characterized by a complex pattern that avoid making lithological predictions or grain size trends using SGR data alone. The three logs contain different "sand:mud" ratio (Log X: 0,42; Log Y: 0,31; Log Z: 0,45) and neither Total GR nor individual elements follow a reliable log motif across Section B.

The origin of SGR vertical trends: climatic control

Numerous studies have successfully correlated the abundance of clay minerals in sedimentary rocks to the ratios of K, Th and U (Myers and Bristow 1989; Slatt *et al.* 1992; Ruffell and Worden 2000). To help calibrate the geochemical variations seen in total GR and K logs along Section A, ten mudstone samples were selected for analysis by x-ray diffraction. The whole rock composition is dominated by quartz (about 32–60%) and clay minerals (37–65%), with minor amounts of K felspar (traces to 1%), plagioclases (1-3%), and calcite in three samples (traces to 2%). The main clay minerals in all ten samples is smectite (45-79%), kaolinite (1-55%), and a single sample contains mixed-layer illite-smectite (99%). Smectite can form from the alteration of volcanic or volcaniclastic material or from a variety of authigenic processes and climatic conditions (Chamley 1989; McKinley *et al.* 2003; Galán 2006), whereas kaolinite is the product of the in situ weathering of precursor clay minerals such as smectite, mica, feldspar, or volcanic material under warm and humid conditions (Senkayi *et al.*1987; Thiry 2000; Sáez *et al.* 2003; Worden and Morad 2003; among others). The single sample containing I/S mixed layer results from moderate chemical weathering under surficial conditions (Chamley 1989) and can take place due to pedogenetic processes under seasonal climates during the transformation of smectite (Wilson 1999; Raucsik and Varga 2008) or from altered volcanic material (Lindgreen and Surlyk 2000; Shoval 2004). X-ray diffraction data indicate that although feldspars are present, clay minerals are volumetrically the most important source in K2O, suggesting that clay mineral distribution and type will be the primary control on K2O distribution in the K log. Higher potassium values in basal levels of S2 sub-unit is probably a result of substitution of K in the structure of smectites before undergoing diagenesis (Drief and Nieto 2000). The upward increase in Al2O3-enriched kaolinite through

Section A (Fig. 7) constitute the likely reason of lower radiation values in both Total GR and K logs, probably reinforced by leaching from feldspars during kaolinite formation (Parkinson 1996). We thus consider that the upward K reduction throughout Section A and the corresponding increase in kaolinite values are associated to increase of paleo-weathering in wet and humid conditions, while the low total GR counts values toward the top of Section A are in such scenario associated to both enhanced continental leaching and changes in clay type. From this, a climatic origin of the identified log motif is proposed.

On the other hand, incorporation of tuffaceous siltstones in floodplain facies of Section B masked the climatic signal and avoid further climatic inferences using SGR data alone.

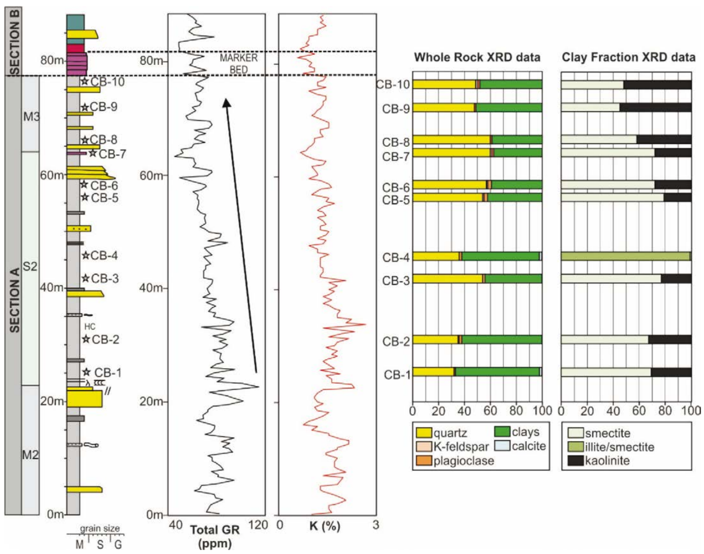

Figure 7. Whole rock and clay-size fraction x-ray diffraction (XRD) data obtained in outcrop SGR Log Z (location in Figure 1C). Quartz and clay minerals are the predominant components. Clay mineral assemblages of the M3 sub-unit are dominated by Al2O3-rich kaolinite, whereas the S2 sub-unit contains more smectite.

PALEOHYDROLOGICAL ESTIMATIONS

The relevant paleohydrological parameters obtained from measurements of cross beds are presented in Table III. Although the calculated values cannot be considered as absolute values, they allow to compare the vertical evolution of the fluvial system, and also provide an independent methodology to be compared with the dataset of channels widths obtained using GPS measurements (see Paredes *et al.*, this congress).

Based in paleohydrological data, channels record an upsection increase in both average flow depth and mean channel width from Section A (d=4.05m; Wc=45.4m) to Section B (d=5.76 m; Wc=69.5m). Mean true width measured using GPS and paleoflow data indicate that channels of

	Section A (n=11)	Section B (n=30)
Cross-set thickness (range, average)	7-30 cm; 18 cm	8-66 cm; 24.5 cm
Mean dune height (h_m) (range, average)	18-88 cm; 52 cm	25-194 cm; 74 cm
Mean Flow Depth (d_m) (range, average)	155-707 cm; 405 cm	432-720 cm; 576 cm
Channel Width (w_c)	45.4 m	69.5 m
Average daily discharge (Qm)	133 m^3/seg	421.59 m^3/seg
Mean bankfull channel depth (d_b)	4.90 m	6.52 m
Bankfull channel width (w_b)	84. 5 m	126.91 m
Average daily discharge (Qm) (2nd method)	53.77 m^3/seg	111.13 m^3/seg
Palaeoslope (S)	0.007847 m/m	0.006344 m/m
Mean bankfull water discharge (Qb)	1748 m^3/seg	4072 m^3/seg
Drainage area (A_d)	23700 km^2	78923 km^2
Principal stream length (L)	525 km	1006 km

Table III. Summary (average) of palaeohydrological data derived from set thickness of cross bedding measured in 41 channels of Sections A and B of the Bajo Barreal Formation. Notice the increasing of channel width in Section B. Flow depth, daily and bankfull discharge also increase in Section B. The equations employed for each parameter can be found in Table II.

Section A are 45.7 m width (n=58), while channels of Section B show a mean true width of 61.1 m (n=160) (Paredes *et al.* this congress), showing a very close correspondence with mean channel width values obtained using paleohydraulics (Table III). Upsection increase in Wc and flow depth reflect larger availability of water into the channel system.

Although calculations of average daily discharge (Qm) using two independent methods show large disparity in the absolute values (see Table III), both approaches show that the resulting Qm values for channels of Section B are larger than those obtained for Section A. As discharge values reflect the size of the catchment area (Van der Neut and Ericksson 1999), it is inferred that larger rivers on an increasingly broad fluvial system developed upward; stream power would also increase along with an enhanced volume of water derived from the larger catchment area (Ad).

Moreover, paleoslope (S) estimations were very close to the maximum gradient of 0.0070 m m-1 for rivers proposed by Blair and McPherson (1994), but far of the 0.026 m m-1 value for modern alluvial fans. Furthermore, the resulting parameters for drainage area (Ad) show a ~ 3 times increase in the catchment area of rivers of Section B in relation to those of Section A. Such increase could be associated to stream capture or enlargement of the drainage basin and would be the main reason of the change in the provenance of the fine-grained components delivered via wash load to the distal floodplain, which in Section B is entirely volcaniclastic.

From this, we have found strong evidence that the vertical increase in the channel proportion and larger connectivity of clastic facies are associated to the occurrence of deeper and wider channels, triggered by a climatic shift toward more humid and wetter conditions.

CONCLUDING REMARKS

By the first time in the exploration history of the Golfo San Jorge basin, three outcrop SGR logs recorded using a portable SGR device has allowed to confidently correlate outcrop exposures of the Bajo Barreal Formation in the Cerro Ballena anticline with specific subsurface intervals in the oilfields. At the outcrops, two distinctive log motifs identified in the Section A, associated to upward reduction in K values and Total GR counts, were confidently correlated to several wells of the Cerro Wenceslao oilfield, involving packages of similar thickness. Based in the large areal distribution of these trends, we interpreted that this log motif represents an increase in the chemical weathering rate associated to leaching of K upward in the Section A. The upward reduction throughout Section A parallel with an increase of the kaolinite content identified by XRD, which constitute strong evidence of a climatic shift toward more humid and wetter climatic conditions upward. Moreover, paleohydrological parameters obtained from 41 channels of Section A and Section B confirm an upward increase in channel depth and width of the channels, with a corresponding increase in discharge and scale of the drainage network, which demonstrate using an independent method larger availability of water upward in the Cerro Ballena exposures.

The set of methodologies demonstrate a climatic origin of the SGR trends, and bring a new approach in order to understand the origin of stacking pattern styles of fluvial successions in the subsurface of the basin. According to our results, changes in the stacking pattern from isolated channels in Section A to densely-stacked channel belts in the Section B are associated to climatic changes, and not to coeval changes in subsidence or base level variation.

The overall shape of the K and Total GR log is similar in fine-grained materials, indicating that K-bearing minerals are responsible for the majority of the total gamma radiation from these rocks. In sandstones and conglomerates the U is the main contributor to the total radioactivity, likely associated to diagenetic processes or fluid migration. The generally weak correlation between elements (K-U-Th) suggest that the sum radioactivity is sourced from multiple mineral carriers, and implies a broad compositional variation within the Bajo Barreal Formation. We demonstrate that outcrop gamma-ray logging could be a quick and rapid tool to characterize sedimentary rocks in the field, to compare this data with subsurface well information, and to determine their suitability as analogues.

ACKNOWLEDGMENTS

We would like to thank SINOPEC ARGENTINA E&P for permission to publish the results. The authors are indebted to landowners of estancia Cañadon Vasco (family Bain) for access to outcrops. This research was partially supported by the Agencia Nacional de Promoción Científica y Tecnológica (PICT 2012-1369). The comments of reviewers Eduardo Breda and Martin M. Paris helped to improve the quality of the final version.

REFERENCES CITED

Acuña, C., A. Schiuma, D. Parra, C. Droeven, M. Beredo and J.M. Paredes, 2011, Modelo paleoambiental de la Formación Mina del Carmen en el Yacimiento Cerro Dragón, Cuenca del Golfo San Jorge, Argentina. VIII Congreso de Exploración de Hidrocarburos, Trabajos Técnicos, p. 419-439. Mar del Plata.

Aigner, T., M. Schaurer, W.D. Junghans and L. Reinhardt, 1995, Outcrop gamma-ray logging and its applications: examples from the German Triassic. Sedimentary Geology, 100: 47-61.

Anderson, R.F., A.P. LeHuray, M.Q. Fleisher and J.W. Murray, 1989, Uranium deposition in the Saanich Inlet sediments, Vancouver Island. Geochimica et Cosmochimica Acta, 53: 2205-2213.

Archangelsky, S., E.S. Bellosi, G.A. Jalfin and C. Perrot, 1994, Palynology and alluvial facies from mid-Cretaceous of Patagonia, subsurface of San Jorge Basin, Argentina. Cretaceous Research, 15: 127-142.

Babek, O., T. Prikryl and J. Hladil, 2007, Progressive drowning of carbonate platform in the Moravo-Silesian Basin (Czech Republic) before the Frasnian/Famennian event: facies, compositional variations and gamma-ray spectrometry. Facies 53 (2), 293-316.

Babek, O., J. Kalvoda, P. Cossey, D. Simícek, F-X. Devuyst and S. Hargreaves, 2013, Facies and petrophysical signature of the Tournaisian/Visean (Lower Carboniferous) sea-level cycle in carbonate ramp to basinal settings of the Wales-Brabant massif, British Isles. Sedimentary Geology, 284-285: 197-213.

Barcat, C., J. Cortiñas, V. Nevistic y H. Zucchi, 1989, Cuenca Golfo San Jorge. In: Chebli G. and L.A. Spalletti (eds.) Cuencas Sedimentarias Argentinas. Universidad Nacional de Tucumán, Serie Correlación Geológica, 6, 319-345.

Blair, T.C. and J.G. McPherson, 1994, Alluvial fans and their natural distinction from rivers based on morphology, hydraulic processes, sedimentary processes, and facies assemblages. Journal of Sedimentary Research, 64: 450-489.

Bridge, J.S. and S.D. Mackey, 1993, A theoretical study of fluvial sandstone body dimensions. In: Flint, S.S. and I.D. Bryant (eds.) Geological modeling of hydrocarbon reservoirs: International Association of Sedimentologists, Special Publication 15, Utrecht, Netherlands, p. 213-236.

Bridge, J.S. and R.S. Tye, 2000, Interpreting the dimensions of ancient fluvial channel bars, channels, and channel belts from wireline-logs and cores. American Association of Petroleum Geologists Bulletin, 84: 1205-1228.

Bridge, J.S., G.A. Jalfin and S.M. Georgieff, 2000, Geometry, lithofacies, and spatial distribution of Cretaceous fluvial sandstone bodies, San Jorge Basin, Argentina: outcrops analog for the hydrocarbon-bearing Chubut Group. Journal of Sedimentary Research 70: 319-337.

Brown, L.F., C. Barcat, L.W. Fisher and A. Nevistic, 1982, Seismic stratigraphic and depositional systems analysis: new exploration approaches applied to the Gulf of San Jorge basin, Argentina. 1st Congreso Nacional de Hidrocarburos, Petróleo y Gas, 127-156. Mar del Plata.

Castillo Gamarra, F., M. Lema and J.M. Paredes, this congress, Spectral gamma-ray logging of Cerro Ballena anticline, Santa Cruz province: Data-driven model for facies classification, with implication for subsurface oilfield development. 10º Congreso de Exploración y Desarrollo de Hidrocarburos, Simposio de Evaluación de Formaciones. Mendoza.

Catuneanu, O., 2006, Principles of Sequence Stratigraphy. Elsevier, Oxford, 375 p.

Chamley, H., 1989, Clay Sedimentology. Springer, Berlin, p. 623.

Corbeanu, R.M., K. Soegaard, R.B. Szerbiak, J.B. Thurmond, G.A. McMechan, D. Wang, S.H. Snelgrove, C.B. Forster and A. Menitove, 2001, Detailed internal architecture of fluvial channel sandstone determined from outcrop and 3-D ground penetrating radar: Example from mid-Cretaceous Ferron Sandstone, east-central Utah: American Association of Petroleum Geologists Bulletin, 85: 1583-1608.

Doveton, J.H., 1994, Geologic log interpretation. SEPM Short Course 29, 1-169.

Drief, A. and F. Nieto, 2000, Chemical composition of smectites formed in clastic sediments. Implications for the smectite-illite transformation. Clay Minerals, 35: 665-678.

Durrance, E.M., 1986, Radioactivity in Geology: Principles and Applications. Ellis Horwood Ltd., Chichester.

Evans, R., A.J. Mory and A.M. Tait, 2007, An outcrop gamma ray study of the Tumblagooda Sandstone, Western Australia. Journal of Petroleum Sciences and Engineering, 57: 37-59.

Figari, E.G., J.J. Hechem and J.F. Homovc, 1990, Arquitectura depositacional de las “Areniscas Verdes” de la Formación Bajo Barreal, provincia del Chubut, Argentina. 3rd Reunión Argentina de Sedimentología, 1: 130-138.

Figari, E.G., S.F. Courtade, R. Calegari, H. Arroyo and L. Constantini, 1998, Estructura y estratigrafía del Cerro Ballena, Faja Plegada meridional de la Cuenca del Golfo San Jorge. X Congreso Latinoamericano de Geología y VI Congreso Nacional de Geología Económica, Vol. I, 18-23. Buenos Aires.

Figari, E., E.E. Stelkov, G. Laffitte, M. Cid de la Paz, S.F. Courtade, J. Celaya, A. Vottero, P. Lafourcade, R. Martínez, and H. Villar, 1999, Los sistemas petroleros de la Cuenca del Golfo San Jorge: Síntesis estructural, estratigráfica y geoquímica. In: 4th Congreso de Exploración y Desarrollo de Hidrocarburos, pp. 197-237. Buenos Aires.

Fitzgerald, M.G., R.M. Mitchum, M.A. Uliana and K.T. Biddle, 1990, Evolution of the San Jorge Basin, Argentina. American Association of Petroleum Geologists Bulletin,74: 879-920.

Galán, E., 2006, Genesis of clay minerals. In: Berhaya, F., B.K.G. Theng and G. Lagaly, (eds.), Handbook of Clay Science, Developments in Clay Science, vol. 1. Elsevier, The Netherlands, 1129-1162.

Georgieff, S.M. and L. Di Benedetto, 2005, Interpretación y correlación entre cuerpos de areniscas en afloramientos y datos de subsuelo. Formación Bajo Barreal. Yacimiento: Cañadón Vasco, Cuenca del Golfo San Jorge. Repsol-YPF.

Georgieff, S.M., G. Escandon and J. Zambrano, 2009, Proyecto Maurek, Visualización Regional, Modelo Sedimentológico. Cuenca del Golfo San Jorge, Argentina. Halliburton S.A.: 125 pp. Inédito.

Ghasemi-Nejad, E., E.P. Ardakani and A. Ruffell, 2010, Palaeoclimate change recorded in Upper Cretaceous (Albian-Cenmanian) Kazhdumi Formation Borehole SPECTRAL Gamma-Ray Logs, South Pars Gas field, Persian Gulf. Paleogeography, Palaeoclimatology, Palaeoecology, 291: 338-347.

Hampson, G.J., W. Davies, S.J. Davies, J.A. Howell and K.R. Adamson, 2005, Use of spectral gamma-ray data to refine subsurface fluvial stratigraphy: late Cretaceous strata in the Book Cliffs, Utah, USA. Journal of the Geological Society, London, 162: 603-621

Hechem, J.J., 1997, Arquitectura y paleodrenaje del sistema fluvial efímero de la Formación Bajo Barreal, cuenca del Golfo San Jorge, Argentina. In: 1st Congreso Latinoamericano de Sedimentología, Actas 1, 315-323 (Isla Margarita, Venezuela).

Hechem, J.J., J.F. Homovc and E.G. Figari, 1990, Estratigrafía del Chubutiano (Cretácico) en la Sierra de San Bernardo, cuenca del Golfo San Jorge, Argentina. 11th Congreso Geológico Argentino, 3, 173-176. San Juan.

Hladil, J., M. Gersl, L. Strnad, J. Frána, A. Langrová and J. Spisiak, 2006, Stratigraphic variation of complex impurities in platform limestones and possible significance of atmospheric dust: a study with emphasis on gamma-ray spectrometry and magnetic susceptibility outcrop logging (Eifelian-Frasnian, Moravia, Czech Republic). International Journal of Earth Sciences, 95: 703-723.

Jain, R.B., S.P. Hingoraney and J. Singh, 1998, A note on radioactivity in the Lower Jurassic sandstones of Lathi Basin, western Rajasthan (India). Journal of Atomic Mineral Science, 6: 117-125.

Keeton, G.I., M.J. Pranter, R.D. Cole and E.R. Gustason, 2015, Stratigraphic architecture of fluvial deposits from borehole images, spectral-gamma-ray response, and outcrop analogs, Piacense Basin, Colorado. American Association of Petroleum Geologists Bulletin, 99: 1929-1956.

Leclair, S.F., 2002, Preservation of cross strata due to migration of subaqueous dunes: an experimental investigation. Sedimentology, 49: 1157-1180.

Leclair, S.F. and J.S. Bridge, 2001, Quantitative interpretation of sedimentary structures formed by river dunes. Journal of Sedimentary Research, 71: 713-716.

Leeder, M.R., 1973, Fluviatile fining-upwards cycles and the magnitude of palaeochannels. Geological Magazine, 110: 265-276.

Legarreta, L., M. Uliana, C.A. Larotonda and G.R. Meconi, 1993, Approaches to nonmarine sequence stratigraphy – theoretical models and examples from Argentine basins. In: Eschard, R. and B. Doliez (eds.), Subsurface Reservoir Characterization from Outcrop Observations. Collection Colloques et Séminaires, vol. 51. Editions Technip, Paris, pp. 125-145.

Leopold, L.B., G.M. Wolman and J.P. Miller, 1964, Fluvial Processes in River Geomorphology. Freeman, San Francisco. 522 pp.

Lesta, P. and R. Ferello, 1972, Región Extraandina del Chubut y norte de Santa Cruz. In: Leanza A. (ed.) Geología Regional Argentina, pp. 601-654. Academia Nacional de Ciencias. Córdoba.

Lindgreen, H. and F. Surlyk, 2000, Upper Permian-Lower Cretaceous clay mineralogy of East Greenland: provenance, palaeoclimate and volcanicity. Clay Minerals, 35: 791-806.

Lindqvist, J., 1997, Gamma radiation anomalies in shallow-marine hummocky bedded transgressive sands; Wangaloa Formation (Paleocene), Great South Basin margin (southern New Zealand). Annual Meeting Abstracts–AAPG and SEPM, 6, p. 70.

Lüning, S., J. Wendt, Z. Belka and B. Kaufmann, 2004, Temporal-spatial reconstruction of the early Frasnian (Late Devonian) anoxia in NW Africa; new field data from the Ahnet Basin (Algeria). Sedimentary Geology, 163: 237-264.

McKinley, G.A., M.J. Follows, J. Marshall and S. Fan, 2003, Interannual variability in air-sea O_2 fluxes and the determination of CO_2 sinks using atmospheric O_2/N_2. Geophysical Research Letters, 30: 1101-1104.

Myers, K.J. and C.S. Bristow, 1989, Detailed sedimentology and gamma ray log characteristics of a Namurian deltaic succession, II: gamma ray logging. In: Whateley, M.K.G. and K.T. Pickering (eds.), Deltas: Sites and Traps for Fossil Fuels. Geological Society, Special Publication, 41: 81-88.

Myers, K.J. and P.B. Wignall, 1987, Understanding Jurassic organic-rich mudrocks; new concepts using gamma-ray spectroscopy and palaeo-ecology; examples from the Kimmeridge Clay of Dorset and the Jet Rock of Yorkshire. In: Leggett, J.K. and G.G. Zuffa, (eds.) Marine Clastic Sedimentology; Concepts and Case Studies. Graham & Trotman, London, 172-189.

North, C.P and M. Boering, 1999, Spectral gamma-ray logging for facies discrimination in mixed fluvial–eolian successions: a cautionary tale. American Association of Petroleum Geologists Bulletin, 83: 155-169.

Osmond, J.K. and M. Ivanovich, 1992, Uranium-series mobilization and surface hydrology. In: Ivanovich, M., Harmon, R.S. (Eds.) Uranium-series disequilibrium: applications to Earth. Marine and Environmental Sciences. Clarendon Press, Oxford, p. 259-289.

Osterkamp, W.R. and E.R. Hedman, 1982, Perennial streamflow characteristics related to channel geometry and sediment in the Missouri River basin. Professional Paper U.S. Geological Survey 1242 (37 pp.).

Paredes, J.M., N. Foix, N. and J.O. Allard, 2016, Sedimentology and alluvial architecture of the Bajo Barreal Formation (Upper Cretaceous) in the Golfo San Jorge Basin: outcrop analogues of the richest oil-bearing fluvial succession in Argentina. Marine and Petroleum Geology, 72: 317-335.

Paredes, J.M., N. Foix, J.O. Allard, M.N. Valle and S.R. Giordano, this congress, Alluvial architecture and fluvial style variations determined from outcrops: example from the Cerro Ballena Anticline (Bajo Barreal Formation) of the Golfo San Jorge Basin. 10º Congreso de Exploración y Desarrollo de Hidrocarburos, Sesiones Técnicas. Mendoza.

Parkinson, D.N., 1996, Gamma ray spectrometry as a tool for stratigraphical interpretation: examples from the western European Lower Jurassic. In: Hesselbo, S.P. and D.N. Parkinson (eds.), Sequence Stratigraphy in British Geology. Geological Society, Special Publication, 103: 231-255.

Postma, G. and J.H. Ten Veen, 1999, Astronomically and tectonically linked variations in gamma-ray intensity in late Miocene hemipelagic successions of the eastern Mediterranean. Sedimentary Geology, 128: 1-12.

Raucsik, B. and A. Varga, 2008, Climato-environmental controls on clay mineralogy of the Hettangian-Bajocian successions of the Mecsek Mountains, Hungary: an evidence for extreme continental weathering during the early Toarcian oceanic anoxic event. Palaeogeography, Palaeoclimatology, Palaeoecology, 265: 1-13.

Rider, M.H., 1990, Gamma-ray log shape used as a facies indicator: critical analysis of an oversimplified method. In: Hurst, A., M.A. Lovell and A.C. Morton, (eds.), Geological application of wireline logs: Geological Society of London Special Publication, 48: 27-37. London.

Rider, M.H., 1999, The Geological Interpretation of Well Logs. Whittles Publishing Services, Dunbeath.

Rodríguez, J.F., 1993, La depositación de las areniscas verdes (Formación Bajo Barreal-Cretácico Tardío) y sus implicancias tafonómicas. 12th Congreso Geológico Argentino and 2nd Congreso de Exploración de Hidrocarburos, pp. 194-199. Mendoza.

Rosholt, J.N., 1992, Mobilization and weathering. In: Ivanovich, M. and R.S. Harmon (eds.), Uranium-series disequilibrium: applications to Earth. Marine and Environmental Sciences. Clarendon Press, Oxford, pp. 167-178.

Ruffell, A.H. and R.H. Worden, 2000, Palaeoclimate analysis using spectral gamma ray data from the Aptian (Cretaceous) of southern England and southern France. Palaeogeography, Palaeoclimatology, Palaeoecology, 154: 313-325.

Sáez, A., M. Inglès, L. Cabrera and A. De Las Heras, 2003, Tectonic-palaeoenvironmental forcing of clay-mineral assemblages in nonmarine settings: the Oligocene-Miocene as Pontes Basin (Spain). Sedimentary Geology, 159: 305-324.

Schumm, S.A., 1968, Speculations concerning palaeohydrologic controls of terrestrial sedimentation. Geological Society of America Bulletin 79: 1573-1588.

Secretaría de Energía, 2016, Informe estadístico anual 2016 del sector energético. Ministerio de Energía y Minería. Secretaría de Planeamiento Energético Estratégico, 40p.

Senkayi, A.L., D.W. Ming, J.B. Dixon and L.R. Hossner, 1987, Kaolinite, opal CT, and clinoptilolite in altered tuffs interbedded with lignite in the Jackson Group, Texas. Clays and Clay Minerals, 35: 281-290.

Slatt, R.M., D.W. Jordan, A. D'Agostino and R.H. Gillespie, 1992, Outcrop gamma-ray logging to improve understanding of subsurface well log correlations. In: Hurst, A., C.M. Griffiths and P.F. Worthington (eds.), Geological applications of wireline logs II: Geological Society of London, Special Publication, 65: 3-19.

Svendsen, J.B. and N.R. Hartley, 2001, Comparison between outcrop spectral gamma ray logging and whole rock geochemistry: implications for quantitative reservoir characterization in continental sequences. Marine and Petroleum Geology 18 (6), 657-670.

Šimíček, D., O. Bábek and J. Leichmann, 2012, Outcrop gamma-ray logging of siliciclastic turbidites: separating the detrital provenance signal from facies in the foreland-basin turbidites of the Moravo-Silesian basin, Czech Republic. Sedimentary Geology, 262: 50-64.

Shoval, S., 2004, Deposition of volcanogenic smectite along the southeastern Neo-Tethys margin during the oceanic convergence stage. Applied Clay Science, 24: 299-311.

Thiry, M., 2000, Palaeoclimatic interpretation of clay minerals in marine deposits: an outlook from the continental origin. Earth-Science Reviews, 49: 201-221.

Umazano, A.M., E.S. Bellosi, G. Visconti and R.N. Melchor, 2008, Mechanism of aggradation in fluvial systems influenced by explosive volcanism: an example from the Upper Cretaceous Bajo Barreal Formation, San Jorge Basin, Argentina. Sedimentary Geology, 203: 213-228.

Van der Neut, M. and P.G. Eriksson, 1999, Palaeohydrological parameters of a Proterozoic braided fluvial system (Wilgerivier Formation, Waterberg Group, South Africa) compared with a Phanerozoic example. International Association of Sedimentologists, Special Publication 28. Blackwell Publishing Ltd, Oxford, UK, p. 381-392.

Williams, G.P., 1978, Bank-full discharge of rivers. Water Resources Research, 14: 1141-1154.

Wilson, M.J., 1999, The origin and formation of clay minerals in soils: past, present and future perspectives. Clay Minerals, 34: 7-25.

Worden, H. and S. Morad, 2003, Clay minerals in sandstones. In: Worden, H. and S. Morad (eds.) Minerals cements in sandstones. International Association of Sedimentologists, Special Publication 34. Blackwell Publishing Ltd, Oxford, UK, pp. 3-41.